Chemical Science

rsc.li/chemical-science

ROYAL SOCIETY
OF **CHEMISTRY**

EDGE ARTICLE
Uwe Grether, Marc Nazaré *et al.*
Detection of cannabinoid receptor type 2 in native cells
and zebrafish with a highly potent, cell-permeable
fluorescent probe

Detection of cannabinoid receptor type 2 in native cells and zebrafish with a highly potent, cell-permeable fluorescent probe†

Thais Gazzi,[a] Benjamin Brennecke,[a] Kenneth Atz,[b] Claudia Korn,[b] David Sykes,[cd] Gabriel Forn-Cuni,[e] Patrick Pfaff,[f] Roman C. Sarott, [ID][f] Matthias V. Westphal,[f] Yelena Mostinski,[a] Leonard Mach,[a] Malgorzata Wasinska-Kalwa,[a] Marie Weise,[a] Bradley L. Hoare,[cd] Tamara Miljuš,[cd] Maira Mexi,[cd] Nicolas Roth,[g] Eline J. Koers,[cd] Wolfgang Guba,[b] André Alker,[b] Arne C. Rufer,[b] Eric A. Kusznir,[b] Sylwia Huber,[b] Catarina Raposo,[b] Elisabeth A. Zirwes,[b] Anja Osterwald,[b] Anto Pavlovic,[b] Svenja Moes,[b] Jennifer Beck,[b] Matthias Nettekoven,[b] Irene Benito-Cuesta,[h] Teresa Grande,[h] Faye Drawnel,[b] Gabriella Widmer,[b] Daniela Holzer,[b] Tom van der Wel,[i] Harpreet Mandhair, [ID][j] Michael Honer,[b] Jürgen Fingerle,[b] Jörg Scheffel,[kl] Johannes Broichhagen, [ID][a] Klaus Gawrisch,[m] Julián Romero,[h] Cecilia J. Hillard,[n] Zoltan V. Varga,[mo] Mario van der Stelt,[i] Pal Pacher,[m] Jürg Gertsch,[j] Christoph Ullmer,[b] Peter J. McCormick,[g] Sergio Oddi,[pq] Herman P. Spaink, [ID][e] Mauro Maccarrone,[qr] Dmitry B. Veprintsev,[cd] Erick M. Carreira,[f] Uwe Grether*[b] and Marc Nazaré [ID]*[a]

Despite its essential role in the (patho)physiology of several diseases, CB_2R tissue expression profiles and signaling mechanisms are not yet fully understood. We report the development of a highly potent, fluorescent CB_2R agonist probe employing structure-based reverse design. It commences with a highly potent, preclinically validated ligand, which is conjugated to a silicon-rhodamine fluorophore, enabling cell permeability. The probe is the first to preserve interspecies affinity and selectivity for both mouse and human CB_2R. Extensive cross-validation (FACS, TR-FRET and confocal microscopy) set the stage for CB_2R detection in endogenously expressing living cells along with zebrafish larvae. Together, these findings will benefit clinical translatability of CB_2R based drugs.

[a]*Leibniz-Forschungsinstitut für Molekulare Pharmakologie (FMP), Campus Berlin-Buch, 13125 Berlin, Germany. E-mail: nazare@fmp-berlin.de*

[b]*Roche Pharma Research & Early Development, Roche Innovation Center Basel, F. Hoffmann-La Roche Ltd., 4070 Basel, Switzerland. E-mail: uwe.grether@roche.com*

[c]*Faculty of Medicine & Health Sciences, University of Nottingham, Nottingham NG7 2UH, England, UK*

[d]*United Centre of Membrane Proteins and Receptors (COMPARE), University of Birmingham and University of Nottingham, Midlands, England, UK*

[e]*Leiden University, Einsteinweg 55, 2333 CC Leiden, the Netherlands*

[f]*Laboratorium für Organische ChemieEidgenössische Technische Hochschule Zürich, Vladimir-Prelog-Weg 3, 8093 Zürich, Switzerland*

[g]*William Harvey Research Institute, Barts and the London School of Medicine, Queen Mary University of London, London EC1M 6BQ, England, UK*

[h]*Faculty of Experimental Sciences, Universidad Francisco de Vitoria, Pozuelo de Alarcón, 28223, Madrid, Spain*

[i]*Department of Molecular Physiology, Leiden Institute of Chemistry, Leiden University, 2333 CC Leiden, the Netherlands*

[j]*Institute of Biochemistry and Molecular Medicine, University of Bern, 3012 Bern, Switzerland*

[k]*Dermatological Allergology, Allergie-Centrum-Charité, Department of Dermatology and Allergy, Charité – Universitätsmedizin Berlin, Corporate Member of Freie Universität Berlin, Humboldt-Universität zu Berlin, Berlin, Germany*

[l]*Allergology, Fraunhofer Institute for Translational Medicine and Pharmacology ITMP, Berlin, Germany*

[m]*National Institute on Alcohol Abuse and Alcoholism, National Institutes of Health, Rockville, MD 20852, USA*

[n]*Department of Pharmacology and Toxicology, Neuroscience Research Center, Medical College of Wisconsin, Milwaukee, WI 53226, USA*

[o]*HCEMM-SU Cardiometabolic Immunology Research Group, Department of Pharmacology and Pharmacotherapy, Semmelweis University, 1085 Budapest, Hungary*

[p]*Faculty of Veterinary Medicine, University of Teramo, 64100 Teramo, European, Italy*

[q]*European Center for Brain Research (CERC), Santa Lucia Foundation, 00179 Rome, Italy*

[r]*Department of Biotechnological and Applied Clinical Sciences, University of L'Aquila, 67100 L'Aquila, Italy*

† Electronic supplementary information (ESI) available: Supplementary figures and tables; general synthetic methods; compound synthesis and characterization; molecular docking; *in vitro* pharmacology; fluorescence spectroscopy; TR-FRET kinetic CB_2R binding assay; FACS analysis; time-lapse confocal imaging; *in vivo* zebrafish imaging; NMR spectra; and N-terminal SNAP-hCB2R sequence. CCDC 1923120. For ESI and crystallographic data in CIF or other electronic format see DOI: 10.1039/d1sc06659e

Introduction

Cannabinoid type 1 and 2 receptors (CB_1R and CB_2R) are key transducers of extracellular stimuli in the endocannabinoid (eCB) system, a fundamental lipid signaling network in all vertebrates.[1,2] Kidney, cardiovascular, gastrointestinal, lung, neurodegenerative and psychiatric disorders, along with pain and cancer are linked to eCB impairment.[3-7] While CB_1R is mainly expressed in the central nervous system and to a lesser extent in peripheral tissue, CB_2R is found throughout the periphery and primarily expressed in immune cells.[8,9] Tissue and cell-type specific receptor expression profiles remain largely uncharted because appropriate biological and chemical tools are lacking. This is aggravated by the absence of antibodies sufficiently specific for both human and rodent CB_2R; which even if available would be precluded for use in translational imaging and incapable of intracellular permeation.[10-12] The development of therapies involving novel CB_2R agonists requires understanding of molecular and cellular mechanisms of action,[13,14] thus, chemical probes targeting CB_2R are needed. Herein we report the synthesis of a novel, selective, cell-permeable, high affinity CB_2R-agonist fluorescent probe (Fig. 1A) along with its pharmacological validation.

This is the first directly labeled small molecule probe to preserve binding affinity and agonistic efficacy at both human and mouse CB_2R. The probe is applied and cross-validated using time-resolved fluorescence resonance energy transfer (TR-FRET) by flow cytometry and cellular trafficking studies. We showcase its application with super resolution live cell imaging in native cells and zebrafish.
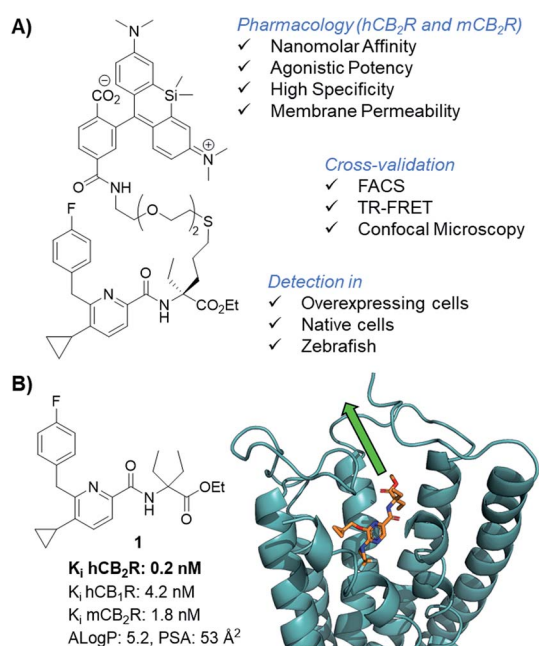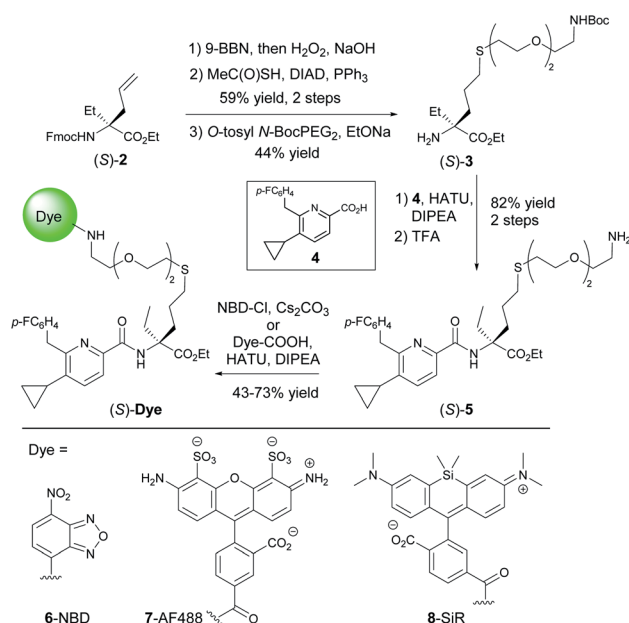
Results and discussion

Probe design, synthesis, and pharmacological characterization

Fluorescent imaging probes have emerged as sensitive tools with high degree of spatiotemporal resolution.[16] Accordingly, we sought to develop a probe that would provide a well-validated translational path from preclinical pharmacological animal data to clinic. In earlier work,[17,18] we described fluorescent probes based on a phytocannabinoid that was lacking desirable pharmacokinetics for translational applications. Accordingly, here we employ a drug-derived, reverse-design approach from a pharmacologically well-validated *in vivo* active compound class that would satisfy a number of desirable boundary conditions: affinity, potency and selectivity, chemical stability, water solubility and membrane permeability.[19,20] A ligand that meets these criteria is **1**,[21-23] displaying picomolar selective binding affinity on human and mouse CB_2R and full agonistic picomolar potency (Fig. 1B and ESI Table S1†). With this as a lead, a conjugation handle was required for fluorophore attachment.

Prospective SAR studies supported by molecular modelling using docking poses of **1** suggested an exit vector (Fig. 1B, green arrow and ESI Tables S2 and 3†) for thioether linked spacers reaching out into the extracellular space, ultimately leading to the design of (*S*)-**5** as a versatile lynchpin (Scheme 1). Its synthesis commenced with hydroboration of (*S*)-**2**, followed by thio-Mitsunobu reaction which allowed linker introduction. The absolute configuration of **2** was assigned by X-ray crystallography of a *N*-toluenesulfonyl-(*S*)-proline derivative (ESI-34, see ESI, S23 and S24†). Following deprotection and coupling, (*S*)-**3** was isolated. Subsequent amide coupling of (*S*)-**3** with acid **4** and deprotection furnished (*S*)-**5**. This compound was used to

Fig. 1 CB_2R agonist **1** for the design of CB_2R-selective fluorescent probe and docking experiments into the co-crystal structure of active state CB_2R with agonist AM12033 (PDB 6KPC).[15]

Scheme 1 Synthesis of probe candidates.

Table 1 Selected pharmacological characteristics of fluoroprobes **6**, **7**, and **8**[a]

Probe	Alog P	K_i [nM]				cAMP EC$_{50}$ [nM] (% efficacy)	
		hCB$_2$R	hCB$_1$R	mCB$_2$R	mCB$_1$R	hCB$_2$R	hCB$_1$R
(S)-**6**-NBD	6.3	9.1	617	33	691	2.2 (72)	>10 000
(R)-**6**-NBD	6.3	159	4925	622	n.d.	17 (84)	>10 000
(S)-**7**-AF488	5.3	44	321	28	>10 000	1.3 (100)	86 (109)
(S)-**8**-SiR	10.6	62	114	117	1892	67 (96)	>10 000

[a] See ESI, S10 for detailed description of the assay protocols.

generate several different probes for study: **6**-NBD, **7**-AF488, and **8**-SiR (Scheme 1). Their pharmacological investigation revealed that all probes displayed high potency, selectivity, and full agonistic properties showing high generality of the probe platform (Table 1 and ESI Table S1†). These CB$_2$R-selective fluorescent probes are the first to preserve interspecies affinity and selectivity for both mouse and human CB$_2$R. Interestingly, (S)-**6**-NBD displayed greater affinity than its enantiomer (Table 1) towards human and murine CB$_2$R. A similar observation was made for fully labeled Alexa Fluor 488 probe pair 7 ((S)-**7** hCB$_2$R K_i: 44 nM *vs.* (R)-**7** hCB$_2$R K_i: 62 nM), where only 1.4-fold *enantio*-discrimination with regard to hCB$_2$R binding affinity favoring the (S)-enantiomer was observed (ESI Table S1†). In particular, NBD probe (S)-**6** and **8**-SiR outperformed with regard to functional selectivity *versus* CB$_1$R (hEC$_{50}$ ratio CB$_1$R/CB$_2$R for (S)-**6**: >4545 and for **8**: >149, Tables 1 and 1†). Consequently, we proceeded with the (S)-enantiomers for our studies. Probe optimization and dye selection were supported by careful evaluation of absorption and emission spectra in buffer (ESI Fig. S3 and Table S6†). In these studies, all probes were observed to be water soluble without any tendency to form aggregates. Broad lipophilicity range of Alog P values was observed, 5.3–10.6 for **7**-AF488 and **8**-SiR, respectively, suggesting good permeability for **8**-SiR which is devoid of negative charges as per our design.

To experimentally probe permeability, the effective permeation coefficients of (R)- and (S)-**6**-NBD were measured in the parallel artificial membrane permeability assay (PAMPA). The fact that both passively permeated through membranes suggested the more lipophilic probe **8**-SiR was likely to be cell-permeable[24] thereby enabling studies of intracellular compartments. Conversely, negatively charged **7**-AF488 was not capable of passive membrane permeation (see ESI, S43†), making it potentially useful in the investigation of extracellular receptor pools. To identify potential off-targets of our labeled ligands, **7**-AF488 probe, having the highest potency, was screened against a customized panel of 50 representative receptors and enzymes. In this assay, ligand **7** exhibited a very clean selectivity profile (ESI Table S4†).

Validation of 8-SiR in overexpressing cells using complementary imaging techniques

To study the specificity of **8**-SiR for human and mouse CB$_2$R, CHO cells overexpressing either hCB$_2$R, mCB$_2$R or hCB$_1$R were incubated at various concentrations and analyzed in FACS experiments (Fig. 2A). In comparison to hCB$_1$R overexpressing cells or WT-CHO control, **8**-SiR was highly specific for CHO cells overexpressing either hCB$_2$R or mCB$_2$R. To confirm ligand specificity and exclude unspecific binding, we investigated whether these compounds can compete for the CB$_2$R binding site with known cold CB$_2$R ligand agonist JWH133 (ref. 25) (Fig. 2B). Following pre-incubation of WT-CHO or hCB$_2$R-CHO cells with these, **8**-SiR efficiently displaced CB$_2$R-agonist JWH133 over a broad concentration range. This illustrates the high degree of target specificity of **8**-SiR in a cellular setting targeting the active conformation of the receptors in its native cellular environment and thereby overruling the observed limited human CB$_1$R/CB$_2$R selectivity ratio in the binding assay by relevant cellular data.[26] Similar high specificity and full displacement by JWH133 was also observed when **7**-AF488 was analyzed in FACS (ESI Fig. S4†).

As previously described by us,[17] we assayed kinetic and equilibrium binding of **8**-SiR *via* TR-FRET (Fig. 2C and D) and further confirmed its use as tracer for TR-FRET applications (see ESI, S16–S20†).

Next, we employed **8**-SiR in confocal microscopy experiments. Currently available CB$_2$R probes require long pre-incubation times (>30 min) in live-cell imaging experiments, contributing to unspecific staining.[27–31] By contrast, we observed instantaneous labeling with **8**-SiR. In accordance with the PAMPA assay (ESI Table S3†), probe **8**-SiR is membrane permeable and successfully entered hCB$_2$R-overexpressing cells, reaching internal receptor pools (Fig. 2E and ESI Video S2†). Besides the cell membrane, labeled hCB$_2$R was detected in intracellular compartments, predominantly within perinuclear structures, reminiscent of Golgi complex and endoplasmic reticulum (see ESI Fig. S4† for higher magnification). Kinetic analysis of the staining of internal membranes with CB$_2$R shows that after 10 minutes saturation had not occurred (Fig. 2G). Moreover, **8**-SiR was nearly non-fluorescent in aqueous environments. This feature allows bright labeling of cellular membranes even in the continued presence of **8**-SiR in culture media,[24,32] which permits imaging over prolonged time periods. Importantly, in hCB$_1$R-overexpressing CHO cells, **8**-SiR did not label the membrane, demonstrating high CB$_2$R-specificity and remarkably low unspecific binding (Fig. 2F and ESI Video S1†). For detection applications, cell-permeable agonist probes have the advantage of accumulating inside cells upon receptor internalization and following recycling events, which consecutively lead to signal amplification, improved image contrast and enhanced detection sensitivity.[33]
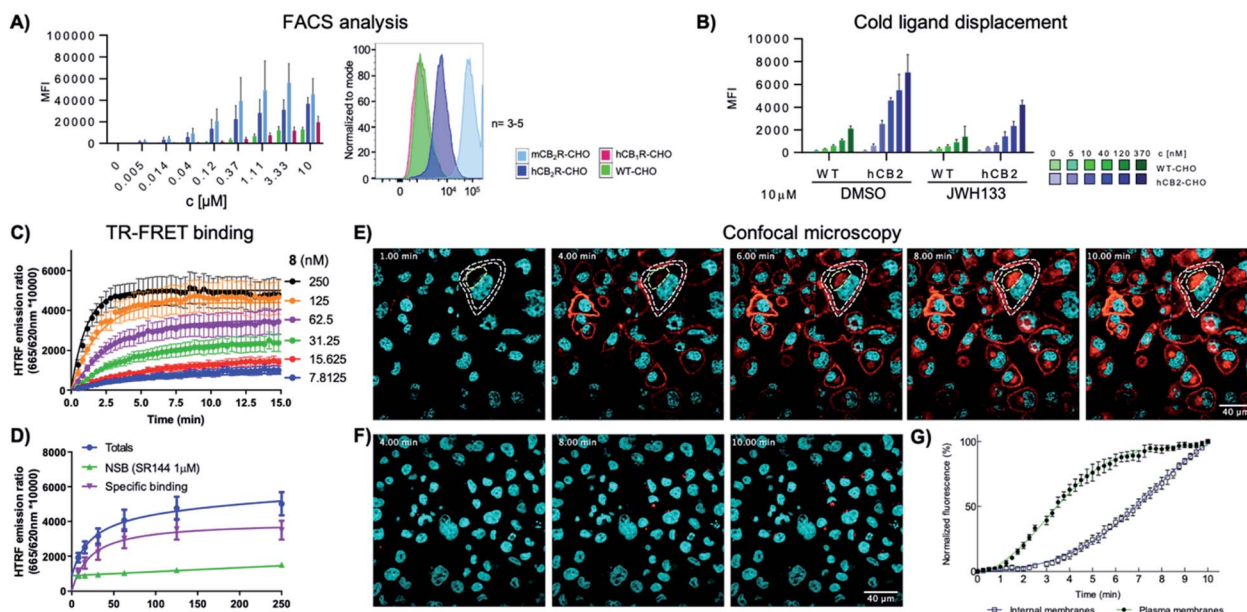
Fig. 2 (A) FACS analysis of the mean fluorescent intensity (MFI) of WT, hCB$_2$R, mCB$_2$R and hCB$_1$R overexpressing CHO cells at different concentrations of **8**-SiR. (B) FACS analysis of the MFI of WT and hCB$_2$R-CHO cells pre-treated with JWH133 (10 μM) and stained with different concentrations of **8**-SiR; see ESI† for details. (C and D) TR-FRET characterization of **8**-SiR binding association (C) and saturation analysis (D) using HEK-hCB$_2$R cell membranes. (E and F) Time-lapse confocal microscopy frames for hCB$_2$R (E) and hCB$_1$R (F). CHO cells co-stained with **8**-SiR (red) and Hoechst 33342 (cyan, nucleus counter stain) at 1, 4, 6, 8 and 10 min; plasma and internal membranes are highlighted with white and yellow dashes, respectively. (G) Association curve of 0.4 μM **8**-SiR on plasma membrane and internal membranes of hCB$_2$R-CHO cells. See also ESI Videos S1 and S2.†

8-SiR enables CB$_2$R visualization in live cells

Finally, the ability of **8**-SiR to visualize endogenous CB$_2$R expression in non-transfected cells was tested (Fig. 3). A challenge in CB$_2$R research is the very low expression level of the receptor in native cells, even when these are known to be responsive to CB$_2$R activation.[34,35] To this end, primary cultures of human macrophages derived from healthy donors and of murine splenocytes from healthy C57BL/6J wild-type mice were isolated. Incubation of primary cell populations with **8**-SiR resulted in increased mean fluorescence (Fig. 3A, B, ESI Videos S3, S4, and S6†).

Consistent with the results obtained previously with CHO-CB$_2$R cells, **8**-SiR produced robust, time-dependent membrane labeling and effected receptor internalization. Probe specificity towards human and mouse CB$_2$R was evident by the abrupt reduction in observed fluorescence after co-incubating cells with **8**-SiR with non-fluorescent JWH133, an agonist with high affinity for human and mouse CB$_2$R[25] (Fig. 3C, D and ESI Videos S5 and S7†). These competition studies demonstrate the capability of probe **8**-SiR for real-time staining of CB$_2$R at native levels with high specificity. Additionally, the excellent cell permeability of **8**-SiR allows accurate tracing of subcellular CB$_2$R receptor distribution and traffic dynamics as well as staining total cellular content of CB$_2$R in real-time, live-cell imaging.

Imaging CB$_2$R *in vivo* using 8-SiR

Having demonstrated the use of **8**-SiR for detection of CB$_2$R in native cells, we then studied the probes in live animals.

Zebrafish embryos and larvae are an established model in biomedical research with high potential for clinical translation[36–38] and show a remarkably high CB$_2$R binding site
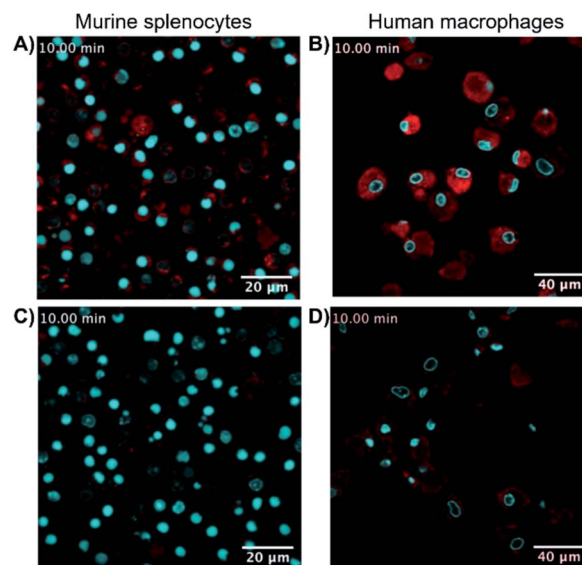

Fig. 3 Super resolution fluorescence microscopy in native cells using probe **8**-SiR. Time-lapse confocal microscopy frames with **8**-SiR in murine splenocytes (A and C) and human macrophages (B and D). Cells were pre-stained with Hoechst 33342 (cyan) to counter stain the nuclei and incubated for 10 min with 0.4 μM **8**-SiR (A and B) or 0.6 μM **8**-SiR and 4 μM JWH133 (C and D). See also ESI Videos S3 to S7.†
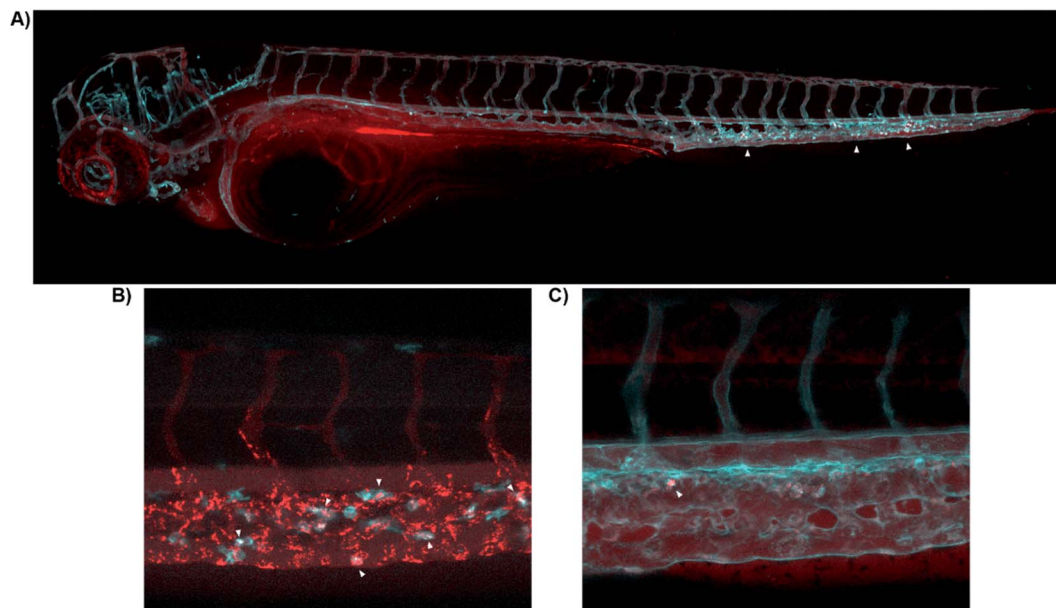
Fig. 4 Real-time *in vivo* visualization of CB$_2$R in zebrafish embryos. (A) **8**-SiR (red) injected in 3dpf Tg(fli1:EGFP) zebrafish larvae, which expresses EGFP fluorescent protein in the blood vasculature (cyan). **8**-SiR was found freely circulating in the blood vasculature after injection, with increased intensity in the CHT region (white triangles). (B) **8**-SiR injected in 3dpf Tg(mpeg1.1:mCherry-F) zebrafish larvae, which expresses mCherry-F fluorescent protein in macrophages (cyan), demonstrating its colocalization. (C) **7**-AF488 (red) injected in 3dpf Tg(kdrl:mCherry) zebrafish larvae, which expresses mCherry fluorescent protein in the blood vasculature (cyan). See also ESI Videos S8 and S9.†

sequence identity to the human receptor[39,40] (ESI Fig. S2†). Probes **7**-AF488 and **8**-SiR were intravenously injected *via* the Duct of Cuvier at 3 days post fertilization (dpf), and their dynamics were analyzed using confocal microscopy (Fig. 4).

Both probes were freely circulating as evidenced by fluorescence within the blood vasculature, which slowly decayed during the first hours post injection due to diffusion throughout the body (Fig. 4A). Over time, probes were extensively taken up at the Caudal Hematopoietic Tissue (CHT), showing as a strong punctate pattern (Fig. 4A). The CHT is a highly perfused tissue wherein hematopoietic stem cells and immune precursors such as macrophages and neutrophils develop during zebrafish embryogenesis.[41] Given CB$_2$R's implication in the immune system,[42–44] we focused on CHT to study the possible uptake of the probes by the residing immune cells.[45,46] However, the CHT is also the residing place for endothelial cells that remove macromolecular waste from the blood *via* scavenging receptors. Analysis revealed uptake of **8**-SiR from motile cells (immune-related) and non-motile (endothelial) cells. Indeed, **8**-SiR colocalized with local residing macrophages prior to its removal from blood circulation *via* endothelial cells (Fig. 4B, and ESI Videos S8 and S9†).

To avoid imaging of binding due to the unspecific scavenging function of endothelial cells, additional analyses were performed during the first 3 hours post injection. These demonstrated specific uptake of **7**-AF488 and **8**-SiR from motile cells both inside CHT as well as crawling into the adjacent fin, putatively endocytosed after contact with CB$_2$R (Fig. 4C and ESI Video S9†). In contrast, injecting the fluorophores without the CB$_2$R recognizing element resulted in unspecific fluorescence signal in all cellular membranes in contact[47] (ESI Fig. S5 and Video S10†).

Conclusions

In conclusion, we have developed cell-permeable, fluorescent probe **8**-SiR, based on a preclinical CB$_2$R agonist **1**. It displays high affinity, specificity, and agonistic potency. Moreover, the probe shows unprecedented, highly consistent interspecies affinity and potency for both human and mouse CB$_2$R. Subsequent to validation in overexpressing systems, the probe was used for imaging in native cells and ultimately in live zebrafish. Specifically, in flow cytometry experiments we labelled CB$_2$R overexpressing cells and demonstrated target specificity by competition experiments. In fluorescence-based TR-FRET assays, kinetic and equilibrium binding profiles for **8**-SiR were determined. Fluoroprobe **8**-SiR was employed to monitor intracellular CB$_2$R distribution in real-time, live-cell imaging by super resolution confocal microscopy with overexpressing hCB$_2$R-CHO cells and endogenously expressing native cells from human macrophages and mouse splenocytes. In zebrafish larvae, **8**-SiR was found to be well tolerated after intravenous injection. It freely circulated inside the blood vasculature over prolonged times before colocalizing with CB$_2$R expressing macrophages. This demonstrates the implementation of the probe *in vivo* and attendant aspects such as biosafety, biodistribution, and cellular uptake.

Probe **8**-SiR provides researchers a unique and novel platform to: (1) overcome the large interspecies differences; (2) access a high specificity and low nanomolar affinity probe for CB$_2$R with full agonist efficacy, and (3) perform an array of biologically and pharmacologically relevant experiments to detect CB$_2$R and study its function. We anticipate that this novel highly translational agonist CB$_2$R fluorescent probe will help to

elucidate CB_2R molecular and cellular mechanisms of action, as well as to unravel its expression levels in different disease states.

Data availability

Primary data for probe synthesis, characterization, photophysical measurements, and fluorescence imaging, as well as atomic coordinates are provided in the ESI.†

Author contributions

M. N., U. G., E. M. C., C. U. and J. F. conceived the research. M. N and U. G. acquired funding for this project. T. G., B. B., D. S., G. F.-C., W. G., A. C. R., N. G., M. H., J. F., K. G., J. R., C. J. H., P. J. MC., M. v. d. S., P. P., J. G., C. U., S. O., H. P. S., M. Ma., H. S., D. B. V., E. M. C., U. G. and M. N. designed the research approach. T. G., B. B, K. A., C. K., D. S., G. F.-C., Y. M., L. M., M. W., R. C. S., M. V. W., P. P., B. L. H., T. M., M. Me., N. R., E. J. K., W. G., A. A., E. A. K., S. H., C. R., E. A. Z., A. O., A. P., S. M., J. B., I. B.-C., F. D., G. W., D. H., T. v. d. W., H. M., Y. S., Z. V. V. G. F.-C, J. S., J. Br. and S. O. performed experiments, analyzed raw data, and worked on probe validation. T. G., C. K., D. S., G. F.-C, S. O., U. G., and M. N. analyzed all data generated, and wrote the manuscript. B. B., K. A., R. C. S., M. V. W., P. P., M. v. d. S., H. P. S., M. Ma., D. B. V., and E. M. C. provided useful comments and feedback for the manuscript. K. G. was not contactable during the submission process of the manuscript, but contributed to the work. All authors have given approval to the final version of the manuscript.

Conflicts of interest

The authors have no conflicts to declare.

Acknowledgements

References

1 S. Munro, K. L. Thomas and M. Abu-Shaar, *Nature*, 1993, **365**, 61–65.

2 W. A. Devane, F. A. Dysarz, M. R. Johnson, L. S. Melvin and A. C. Howlett, *Mol. Pharmacol.*, 1988, **34**, 605–613.

3 P. Pacher and R. Mechoulam, *Prog. Lipid Res.*, 2011, **50**, 193–211.

4 J. Guindon and A. G. Hohmann, *Br. J. Pharmacol.*, 2008, **153**, 319–334.

5 R. P. Picone and D. A. Kendall, *Mol. Endocrinol.*, 2015, **29**, 801–813.

6 A. M. Malfitano, S. Basu, K. Maresz, M. Bifulco and B. N. Dittel, *Semin. Immunol.*, 2014, **26**, 369–379.

7 R. G. Pertwee, *Philos. Trans. R. Soc.*, 2012, **367**, 3353–3363.

8 C. Turcotte, M. R. Blanchet, M. Laviolette and N. Flamand, *Cell. Mol. Life Sci.*, 2016, **73**, 4449–4470.

9 S. Galiegue, S. Mary, J. Marchand, D. Dussossoy, D. Carriere, P. Carayon, M. Bouaboula, D. Shire, G. Le Fur and P. Casellas, *Eur. J. Biochem.*, 1995, **232**, 54–61.

10 H. Y. Zhang, H. Shen, C. J. Jordan, Q. R. Liu, E. L. Gardner, A. Bonci and Z. X. Xi, *Acta Pharmacol. Sin.*, 2019, **40**, 398–409.

11 B. Cecyre, S. Thomas, M. Ptito, C. Casanova and J. F. Bouchard, *Naunyn Schmiedebergs Arch. Pharmacol.*, 2014, **387**, 175–184.

12 Y. Marchalant, P. W. Brownjohn, A. Bonnet, T. Kleffmann and J. C. Ashton, *J. Histochem. Cytochem.*, 2014, **62**, 395–404.

13 D. S. Tyler, J. Vappiani, T. Caneque, E. Y. N. Lam, A. Ward, O. Gilan, Y. C. Chan, A. Hienzsch, A. Rutkowska, T. Werner, A. J. Wagner, D. Lugo, R. Gregory, C. Ramirez Molina, N. Garton, C. R. Wellaway, S. Jackson, L. MacPherson, M. Figueiredo, S. Stolzenburg, C. C. Bell, C. House, S. J. Dawson, E. D. Hawkins, G. Drewes, R. K. Prinjha, R. Rodriguez, P. Grandi and M. A. Dawson, *Science*, 2017, **356**, 1397–1401.

14 G. M. Simon, M. J. Niphakis and B. F. Cravatt, *Nat. Chem. Biol.*, 2013, **9**, 200–205.

15 T. Hua, X. Li, L. Wu, C. Iliopoulos-Tsoutsouvas, Y. Wang, M. Wu, L. Shen, C. A. Johnston, S. P. Nikas, F. Song, X. Song, S. Yuan, Q. Sun, Y. Wu, S. Jiang, T. W. Grim, O. Benchama, E. L. Stahl, N. Zvonok, S. Zhao, L. M. Bohn, A. Makriyannis and Z. J. Liu, *Cell*, 2020, **180**, 655–665.

16 L. A. Stoddart, L. E. Kilpatrick, S. J. Briddon and S. J. Hill, *Neuropharmacology*, 2015, **98**, 48–57.

17 R. C. Sarott, M. Westphal, P. Pfaff, C. Korn, D. A. Sykes, T. Gazzi, B. Brennecke, K. Atz, M. Weise, Y. Mostinski, P. Hompluem, E. Koers, T. Miljus, N. J. Roth, H. Asmelash, M. C. Vong, J. Piovesan, W. Guba, A. Rufer, E. A. Kusznir, S. Huber, C. Raposo, E. A. Zirwes, A. Osterwald, A. Pavlovic, S. Moes, J. Beck, I. Benito-Cuesta, T. Grande, S. Ruiz de Martin, A. A. Yeliseev, F. Drawnel, G. Widmer,

D. Holzer, T. van der Wel, H. Mandhair, C.-Y. Yuan, W. Drobyski, Y. Saroz, N. L. Grimsey, M. Honer, J. Fingerle, K. Gawrisch, J. Romero, C. Hillard, Z. Varga, M. van der Stelt, P. Pacher, J. Gertsch, P. McCormick, C. Ullmer, S. Oddi, M. Maccarrone, D. Veprintsev, M. Nazaré, U. Grether and E. M. Carreira, *J. Am. Chem. Soc.*, 2020, **142**, 16953–16964.

18 M. V. Westphal, R. C. Sarott, E. A. Zirwes, A. Osterwald, W. Guba, C. Ullmer, U. Grether and E. M. Carreira, *Chem.–Eur. J.*, 2020, **26**, 1380–1387.

19 J. Blagg and P. Workman, *Cancer Cell*, 2017, **32**, 9–25.

20 P. Workman and I. Collins, *Chem. Biol.*, 2010, **17**, 561–577.

21 C. Bissantz, U. Grether, P. Hebeisen, A. Kimbara, Q. Liu, M. Nettekoven, M. Prunotto, S. Roever, M. Rogers-Evans, T. Schulz-Gasch, C. Ullmer, Z. Wang and W. Yang, WO2012168350A1, 2012.

22 A. Haider, L. Gobbi, J. Kretz, C. Ullmer, A. Brink, M. Honer, T. J. Woltering, D. Muri, H. Iding, M. Burkler, M. Binder, C. Bartelmus, I. Knuesel, P. Pacher, A. M. Herde, F. Spinelli, H. Ahmed, K. Atz, C. Keller, M. Weber, R. Schibli, L. Mu, U. Grether and S. M. Ametamey, *J. Med. Chem.*, 2020, **63**, 10287–10306.

23 A. Haider, J. Kretz, L. Gobbi, H. Ahmed, K. Atz, M. Burkler, C. Bartelmus, J. Fingerle, W. Guba, C. Ullmer, M. Honer, I. Knuesel, M. Weber, A. Brink, A. M. Herde, C. Keller, R. Schibli, L. Mu, U. Grether and S. M. Ametamey, *J. Med. Chem.*, 2019, **62**, 11165–11181.

24 G. Lukinavičius, K. Umezawa, N. Olivier, A. Honigmann, G. Yang, T. Plass, V. Mueller, L. Reymond, I. R. Corrêa Jr, Z. G. Luo, C. Schultz, E. A. Lemke, P. Heppenstall, C. Eggeling, S. Manley and K. Johnsson, *Nat. Chem.*, 2013, **5**, 132–139.

25 M. Soethoudt, U. Grether, J. Fingerle, T. W. Grim, F. Fezza, L. de Petrocellis, C. Ullmer, B. Rothenhausler, C. Perret, N. van Gils, D. Finlay, C. MacDonald, A. Chicca, M. D. Gens, J. Stuart, H. de Vries, N. Mastrangelo, L. Xia, G. Alachouzos, M. P. Baggelaar, A. Martella, E. D. Mock, H. Deng, L. H. Heitman, M. Connor, V. Di Marzo, J. Gertsch, A. H. Lichtman, M. Maccarrone, P. Pacher, M. Glass and M. van der Stelt, *Nat. Commun.*, 2017, **8**, 13958–13972.

26 The binding data are generated from previously frozen membranes, while flow cytometry experiments are performed with viable cells. We hypothesize that membrane lysate preparation affects CB$_2$R and CB$_1$R structure differentially, with detrimental effects on the observed selectivity. In the cAMP assay, which is also performed on living cells, the behaviour is consistently similar to that in flow cytometry, confocal imaging. Therefore, in the subsequent much more relevant multiple whole cell evaluations targeting the agonist binding site in its native conformation we observed consistently a very high selectivity.

27 S. Singh, C. R. M. Oyagawa, C. Macdonald, N. L. Grimsey, M. Glass and A. J. Vernall, *ACS Med. Chem. Lett.*, 2019, **10**, 209–214.

28 F. Spinelli, R. Giampietro, A. Stefanachi, C. Riganti, J. Kopecka, F. S. Abatematteo, F. Leonetti, N. A. Colabufo, G. F. Mangiatordi, O. Nicolotti, M. G. Perrone, J. Brea, M. I. Loza, V. Infantino, C. Abate and M. Contino, *Eur. J. Med. Chem.*, 2020, **188**, 112037.

29 S. Zhang, P. Shao and M. Bai, *Bioconjugate Chem.*, 2013, **24**, 1907–1916.

30 X. Ling, S. Zhang, P. Shao, W. Li, L. Yang, Y. Ding, C. Xu, N. Stella and M. Bai, *Biomaterials*, 2015, **57**, 169–178.

31 R. R. Petrov, M. E. Ferrini, Z. Jaffar, C. M. Thompson, K. Roberts and P. Diaz, *Bioorg. Med. Chem. Lett.*, 2011, **21**, 5859–5862.

32 L. Wang, M. S. Frei, A. Salim and K. Johnsson, *J. Am. Chem. Soc.*, 2019, **141**, 2770–2781.

33 F. Reynolds and K. A. Kelly, *Mol. Imaging*, 2011, **10**, 407–419.

34 A. Cooper, S. Singh, S. Hook, J. D. A. Tyndall and A. J. Vernall, *Pharmacol. Rev.*, 2017, **69**, 316–353.

35 N. L. Grimsey, C. E. Goodfellow, M. Dragunow and M. Glass, *Biochim. Biophys. Acta*, 2011, **1813**, 1554–1560.

36 M. C. Gomes and S. Mostowy, *Trends Microbiol.*, 2020, **28**, 10–18.

37 E. E. Patton and D. M. Tobin, *Dis. Models Mech.*, 2019, **12**, dmm039370.

38 E. E. Patton, L. I. Zon and D. M. Langenau, *Nat. Rev. Drug Discovery*, 2021, **20**, 611–628.

39 R. G. Krug II and K. J. Clark, *Gene*, 2015, **570**, 168–179.

40 F. Oltrabella, A. Melgoza, B. Nguyen and S. Guo, *Dev., Growth Differ.*, 2017, **59**, 194–210.

41 E. Murayama, K. Kissa, A. Zapata, E. Mordelet, V. Briolat, H.-F. Lin, R. I. Handin and P. Herbomel, *Immunity*, 2006, **25**, 963–975.

42 V. Esain, W. Kwan, K. J. Carroll, M. Cortes, S. Y. Liu, G. M. Frechette, L. M. Sheward, S. Nissim, W. Goessling and T. E. North, *Stem Cells*, 2015, **33**, 2596–2612.

43 Y. J. Liu, H. B. Fan, Y. Jin, C. G. Ren, X. E. Jia, L. Wang, Y. Chen, M. Dong, K. Y. Zhu, Z. W. Dong, B. X. Ye, Z. Zhong, M. Deng, T. X. Liu and R. Ren, *J. Biol. Chem.*, 2013, **288**, 13551–13562.

44 I. Rodriguez-Martin, M. J. Herrero-Turrion, E. Marron Fdez de Velasco, R. Gonzalez-Sarmiento and R. E. Rodriguez, *Gene*, 2007, **389**, 36–44.

45 G. Arias-Alpizar, B. Koch, N. M. Hamelmann, M. A. Neustrup, J. M. J. Paulusse, W. Jiskoot, A. Kros and J. Bussmann, *Nanomedicine*, 2021, **34**, 102395.

46 F. Campbell, F. L. Bos, S. Sieber, G. Arias-Alpizar, B. E. Koch, J. Huwyler, A. Kros and J. Bussmann, *ACS Nano*, 2018, **12**, 2138–2150.

47 M. Guarin, R. Faelens, A. Giusti, N. De Croze, M. Leonard, D. Cabooter, P. Annaert, P. de Witte and A. Ny, *Sci. Rep.*, 2021, **11**, 12229.